Astro Ltd.

LETTER

Random laser emission from a Rhodamine B-doped GPTS/TEOS-derived organic/silica monolithic xerogel

View the article online for updates and enhancements.

Related content

Recent citations

IOP ebooks™

Bringing you innovative digital publishing with leading voices to create your essential collection of books in STEM research.

Start exploring the collection - download the first chapter of every title for free.

Letter

Random laser emission from a Rhodamine B-doped GPTS/TEOS-derived organic/silica monolithic xerogel

Luis M G Abegão[1], **D S Manoel**[2], **A J G Otuka**[4], **P H D Ferreira**[3], **D R Vollet**[2], **D A Donatti**[2], **L De Boni**[4], **C R Mendonça**[4], **F S De Vicente**[2], **J J Rodrigues Jr**[1] **and M A R C Alencar**[1,5]

[1] Departamento de Física, Universidade Federal de Sergipe, 49.100-000, São Cristóvão, SE, Brazil
[2] Departamento de Física, Unesp—Universidade Estadual Paulista, 13506-900, Rio Claro, SP, Brazil
[3] Departamento de Física, Universidade Federal de São Carlos, 13565-905, São Carlos, SP, Brazil
[4] Instituto de Física de São Carlos, Universidade de São Paulo, CP 369, 13560-970, São Carlos, SP, Brazil

E-mail: marca.ufs@gmail.com

Abstract

A Rhodamine B-doped 3-glycidoxypropyltrimethoxysilane (GPTS)/tetraethyl orthosilicate (TEOS)-derived organic/silica monolithic xerogel with excellent optical properties was prepared and its potential as a random laser host investigated. This hybrid material has a non-porous organic/inorganic morphology with silica-rich nanoparticles of less than 10 nm in diameter homogeneously dispersed within the matrix. Random laser emission with incoherent feedback, centered at 618 nm, was observed from Rhodamine B incorporated into the monolithic xerogel when excited by a 532 nm pulsed laser. This hybrid system is shown to be very promising for the development of a new class of random laser-based integrated devices, with applications ranging from optical bio-imaging to sensing.

Keywords: random laser, silica nanoparticles, organic–inorganic hybrid material, incoherent feedback

(Some figures may appear in colour only in the online journal)

1. Introduction

Hybrid organic–inorganic materials (HOIMs) are among the most promising media for optical and photonic applications [1–3]. By combining the peculiar chemical and physical properties of such distinct compounds, it is possible to produce a composite material with optimized optical properties in comparison with the individual original media. For instance, it is possible to enhance the nonlinear optical responses of an organic material by adding a small number of inorganic nanoparticles into it; however, it is necessary to

reduce the impact of any undesirable effects that this inclusion may cause [4]. Hybrid organic–inorganic media, such as organic lead halide perovskite materials, present improved electronic and optical properties and they have been developed for use in several photonic applications [5]. By exploiting the versatility of organic polymers, different strategies have been employed aiming the production of improved photonic hybrid devices [6].

Among the multitude of optical and photonics applications based in HOIM, the appropriate combination of organic dyes and inorganic structures and/or nanoparticles have been intensively investigated for use in random laser (RL) systems [7–10]. In this class of device, there is no mirror in the optical

[5] Author to whom any correspondence should be addressed.

cavity. Instead, the feedback mechanism that allows light amplification by stimulated emission of radiation through the gain medium is light scattering, which is intrinsically random [11–13].

Interest in these systems has increased enormously over the past two decades, although they were proposed originally by Ambartsumyan and coworkers in 1966 [14]. Owing to their peculiar properties, RLs have been used as benchmarks for investigating fundamental effects. For instance, one of the most fundamental paradigms of statistical mechanics is replica theory, for which so-called replica symmetry breaking was not experimentally demonstrated until the use of RLs [15, 16]. Another example is the experimental observation of a stochastic process called the Lévy fluctuation using an RL [17] and the verification of light localization in amplifying disordered media [18]. In addition, RLs have proven to be useful in several applications where their low coherence can be exploited for imaging applications, such as light projector systems [19] and time-resolved microscopy [20], due to their speckle suppression. An RL can also be used to measure milk fat content [21], to determine low concentrations of dopamine [22], as a tool for cancerous tissue diagnosis [23], among other applications [12, 13].

Furthermore, research conducted over the last few decades has focused on new sol–gel-derived organic/silica hybrid materials, which present several advantages for the design and application of materials for optics and photonics [24]. Different solid-state hybrid organic/inorganic systems have been investigated as RL media [25–29]. Nevertheless, the development of a low-cost RL material, with improved characteristics and optical integration capabilities, is a very important issue that must be overcome in order to make RL devices competitive commercial products. Indeed, combining the properties of the organic/inorganic hybrid matrices with the functionality of organic molecules yields the next generation of multifunctional materials, which have been recognized to possess a wide spectrum of properties with applications in several fields [30].

In this context, the development of HOIM via the sol–gel process is a promising approach for the design of RL materials due to the ease of obtaining silica-based dense bulks, with the possibility of doping with organic and/or inorganic components. Laser properties have been reported for silica gel doped with Rhodamine 6G and Rhodamine B [31], 3-glycidoxypropyltrimethoxysilane (GPTS)-based hybrids with Titania and Rhodamine 6G [32], and distributed-feedback dye-doped sol–gel silica lasers using periodic gain modulation [33]. Efficient RL emission has been also demonstrated for di-ureasil-based hybrids incorporating Rhodamine 6G [34]. RL action was also reported for a silica gel containing SiO_2 nanoparticles embedding Rhodamine 6G [35]. Furthermore, in a recent study, the combination of tetraethyl orthosilicate (TEOS) and GPTS, with embedded luminescent quantum dots, presented enhanced emission quantum efficiency [36]. Also, femtosecond laser fabrication of waveguides in monolithic xerogels of GPTS/TEOS-derived organic/silica hybrids doped with Rhodamine B has been demonstrated recently [37].
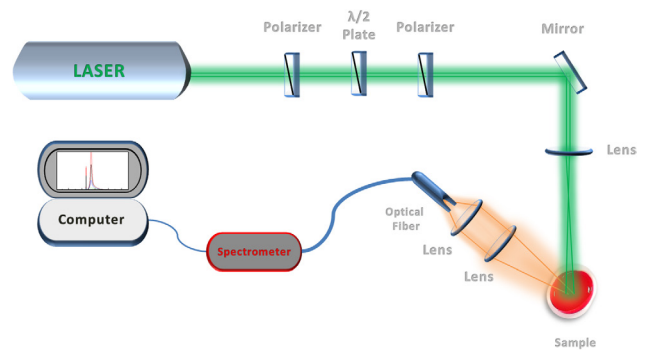

Figure 1. Schematic view of the luminescence RL setup.

In this work, we report random lasing in Rhodamine B-doped GPTS/TEOS-derived organic/silica monolithic xerogels prepared by a sol–gel process. In this system, light scatters are silica-rich nanometric domains within the GPTS/TEOS-derived xerogel. The intrinsic nanometric structure of the material was characterized by transmission electron microscopy (TEM) and the light scattering mean-free path due to the silica-rich nanoparticles was estimated. Laser-induced luminescence experiments were carried out and the system's RL emission was observed and analyzed.

2. Experiments and results

By using a sol–gel process, Rhodamine B-doped GPTS/TEOS-derived monolithic xerogel (RB-doped xerogel) samples were prepared by acid hydrolysis of GPTS (Aldrich 98%) and TEOS (Aldrich 99%) compounds, dissolved in ethanol (EtOH). Additionally, for acid-catalyzed hydrolysis, a solution of HNO_3 in water (0.6 M) was slowly dropped into the alkoxide mixtures. The molar ratio for GPTS/TEOS/EtOH/H_2O/HNO_3 used in the hydrolysis was approximately 1:1:3:7:0.1. The undoped sols were refluxed at 80 °C for 24 h under mechanical stirring, allowing complete hydrolyzation and producing a very stable and clear organic/ailica hybrid sol with a 1:1 GPTS/TEOS ratio. Ethanolic solutions with a Rhodamine B concentration of 25 mmol l^{-1} were prepared by dissolving Rhodamine B powder (for fluorescence; Sigma-Aldrich) in ethanol. In the following step, 20 ml of GPTS/TEOS-derived organic/silica sols were doped with 5 ml of Rhodamine B ethanolic solution. Bulks of RB-doped xerogel with a Rhodamine B concentration of 19.3 mmol l^{-1} were obtained after very slow drying of a known volume of the Rhodamine B-doped sol in sealed flasks at 40 °C. Density of the monolithic xerogels was measured (1.395 g cm^{-3}) by using the Archimedes method, thereby allowing a precise determination of the Rhodamine B concentration in the samples. The RB-doped xerogels were optically clear, free of cracks and did not present any porosity when measured by nitrogen adsorption. The fluorescence spectra of the produced RB-doped xerogel sample were also recorded using a Varian Cary Eclipse fluorescence spectrophotometer.

The GPTS/TEOS-derived organic/silica sol doped with Rhodamine B was prepared for TEM imaging by drying a drop of the respective sol on a copper grid coated with a thin
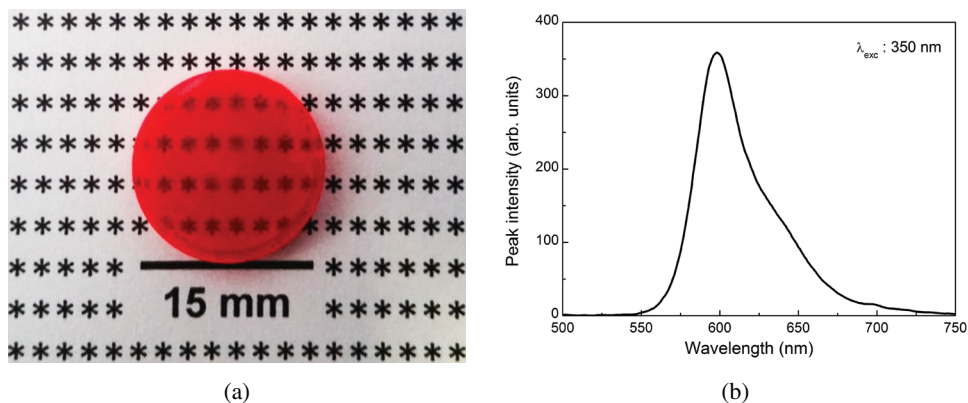
(a)

(b)

Figure 2. (a) Photograph of the RB-doped GPTS/TEOS-derived monolithic xerogel with a concentration of 19.3 mmol l^{-1} and (b) its fluorescence spectrum at room temperature.
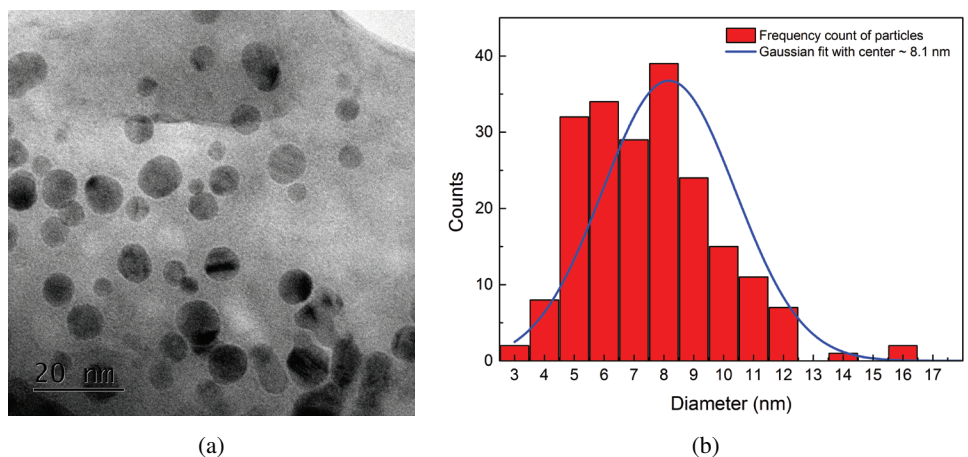

(a)

(b)

Figure 3. (a) TEM image showing silica-rich particles dispersed in the RB-doped GPTS-TEOS-derived organic/silica hybrid and (b) particle size distribution with a Gaussian fit.
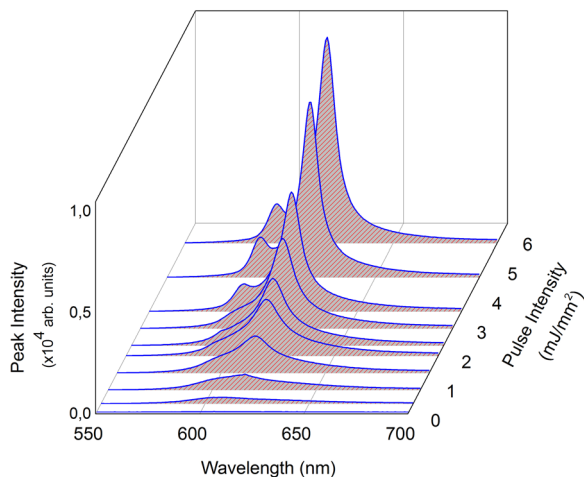

Figure 4. Emission spectra evolution as a function of the pump fluence.

layer of carbon. The TEM images were made using a JEM-1400 PLUS from JEOL, operated at an acceleration voltage of 120 keV, and a megapixel (2048 × 2048) bottom-mount CCD camera for retrieving high-resolution images, which were processed and analyzed by software to quantify particle size distribution.

For RL studies, the experimental luminescence setup presented in figure 1 was employed. The excitation source was the second harmonic of a Nd:YAG pulsed laser (8 ns time duration at 10 Hz repetition rate), model Vibrant 355 II from OPOTEK. The incident pulse energy over the sample was continuously controlled by a set of half-wavelength plates and two polarizers. The light beam was focused by a 20 cm convergent lens. We could vary the sample position along the light beam path. The incidence angle on the excitation beam was about 45°. The emitted light was collected normally to the sample surface by a set of lenses and coupled to an optical fiber which was connected to a CCD-compact spectrometer, model QE65000 from OceanOptics.

The bulk used to investigate RL properties was doped with 19.3 mmol l^{-1} of Rhodamine B (RB). Figure 2(a) shows a photograph of a typical RB-doped xerogel of approximately 3 mm in thickness produced by the sol–gel process. As can be observed in figure 2(a), transmitted light through the sample indicates that a weak light scattering process occurs inside the xerogel. Figure 2(b) displays the characteristic fluorescence spectrum of this RB as the gain medium on the hybrid system, measured using the 350 nm laser excitation wavelength of a fluorescence spectrophotometer, which presented a maximum intensity around 600 nm.
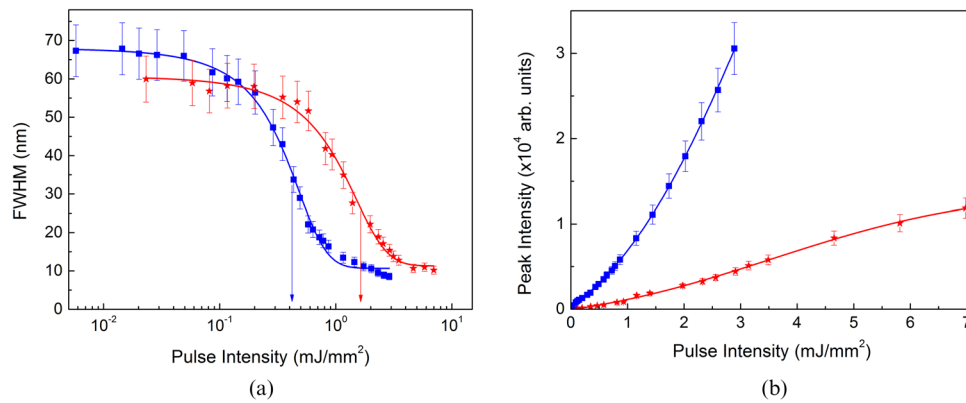
Figure 5. (a) FWHM in log scale and (b) emission peak intensity in linear scale for RB-doped xerogel with two excitation spot sizes of 1.66 mm (squares) and 0.74 mm (stars). The solid lines are just a guide to the eyes.

Figure 3(a) shows the TEM image of the RB-doped hybrid sample revealing the presence of nanoparticles dispersed within the matrix. Analyzing figure 3(a), we can observe two phases: the brightest areas, which correspond to a lower density phase, indicate a homogeneous polymer-rich phase, while the nearly circular darkest areas evidence formation of nanoparticles rich in silica, which possess higher density. For comparison, the density of amorphous SiO_2 is 2.2 g cm^{-3} and the density of the organic radical (R) propyl glycidyl ether from the GPTS precursor is $\approx$1.0 g cm^{-3}.

Density of the RB-doped xerogel was measured (1.395 g cm^{-3}) by using the Archimedes method and the result is in good agreement with the calculated density (1.370 g cm^{-3}), considering the density of the individual constituents of the organic/silica hybrid matrix and the inexistence of porosity as measured by nitrogen adsorption. Combining these results with the molar weight of the solid sample and its individual constituents (SiO_2 and $SiO_{3/2}$–R), one can estimate the volume fraction occupied by the SiO_2 as being approximately 31%, while the organic phase formed from the radical R fills the remaining volume (around 69%).The Gaussian distribution of particle size was obtained by measuring particle diameters, revealing the center of its Gaussian fit at 8.1 nm, as shown in figure 3(b).

The formation of Si–O–Si bonds reduces the entropy of the system and promotes self-organization at a molecular level. Silica self-organization occurs through van der Waals interactions and it is favored by polycondensation, leading to the formation of very small primary particles which grow by aggregation [38, 39].

The early stage of formation and growth of silica-rich domains in sols of GPTMS-TEOS-derived organic/silica hybrids was studied *in situ* during the condensation process by small angle x-ray scattering (SAXS) [40]. Also, dispersed silica-rich nanostructured domain formation was observed in GPTS-TEOS-epoxy-derived hybrid films [41] and in PEO-TEOS-derived nanocomposites [40]. Furthermore, silica-rich nanocrystal formation was reported in a basic sol derived from GPTMS organosilane [42].

Regarding the silica nanoparticles in the RB-doped xerogel, the number of particles by volume of solid matrix can

be estimated using the spherical volume of 8.1 nm diameter and the volume fraction occupied by the SiO_2. We have obtained that the silica nanoparticle concentration was $\rho = 1.11 \times 10^{18}$ cm^{-3}. The sample scattering cross section of one silica sphere of $\approx$8.1 nm in diameter at 618 nm was calculated to be equal to 9.46×10^{-22} cm^2. Using these quantities and considering the refractive index of silica and RB-doped xerogel to be 1.458 [43] and 1.492 [44], respectively, the scattering mean-free path of this hybrid system could be estimated using Rayleigh theory as $l_s = (\rho\sigma_s)^{-1} = 9.52 \times 10^2$ cm.

A similar broadband spectrum, as shown in figure 2(b), was also obtained when RB-doped xerogel was excited at 532 nm by a nanosecond pulsed laser, with pulse energy smaller than 1 mJ. As shown in figure 4, at low pumping energy, only spontaneous emission, characterized by the fluorescence spectral band with a maximum at $\lambda \approx 600$ nm, can be observed. However, despite the weak scattering, as the incident energy was raised, the emission spectrum was strongly modified. One can clearly see that the second band around 620 nm increases faster than the remaining fluorescence spectrum, evolving into a dominant narrowband emission at higher excitation energies. It is worth mentioning that no sharp spikes were observed in the measured spectra, even at single pulse excitation.

Two excitation-dependent spectral features have been used to identify and characterize RLs which employ organic dyes as amplifying media: an abrupt increase in emission intensity and a drastic reduction on the fluorescence linewidth as the pump energy is raised. Both quantities were monitored and analyzed for the fluorescence exhibited by the RB-doped xerogel. In figures 5(a) and (b), the full-width half-medium (FWHM) and the peak intensity are presented, respectively, as observed for the band centered at 618 nm as a function of the excitation energy. From the peak intensity behavior, a significant change of the curve slope can be observed. At the same time, the FWHM of this band is reduced smoothly from $\approx$65 nm to $\approx$10 nm.

Using the value of the medium-scattering mean-free path, we calculated the product $k \times l_s$ for this system to be roughly 9.68×10^7, which is comparable with other RL systems

investigated previously that operate in a very weak scattering regime [45–47]. In order to ensure that it was RL emission, the threshold pump intensity must have changed if the excitation spot size varied [48]. Figure 5(a) clearly shows a difference between the FWHM thresholds from two different excitation spot sizes. The spot size diameters used were 1.66 mm and 0.74 mm, and the thresholds obtained were 0.4 mJ mm^{-2} and 1.7 mJ mm^{-2}, respectively.

3. Conclusions

In conclusion, we have demonstrated that RB-doped GPTS/TEOS-derived organic/silica monolithic xerogel exhibits incoherent RL emission in a weakly scattering system. This system presented an FWHM of around 65 nm at low pumping energies ($<$1 mJ) and for higher pumping energies ($>$3 mJ) the system could achieve a FWHM around 10 nm. The observed RL emission, as well as the good optical quality of the produced samples and the possibility of optical waveguide production within this medium, indicates that this hybrid material is a very promising platform for the development of integrated optical systems.

Aknowledgment

References

[1] Clark J and Lanzani G 2010 Organic photonics for communications *Nat. Photon.* **4** 438–46

[2] Kao T S *et al* 2016 Controllable lasing performance in solution-processed organic–inorganic hybrid perovskites *Nanoscale* **8** 18483–8

[3] Lebeau B and Innocenzi P 2011 Hybrid materials for optics and photonics *Chem. Soc. Rev.* **40** 886–906

[4] Lal S, Link S and Halas N J 2007 Nano-optics from sensing to waveguiding *Nat. Photon.* **1** 641–8

[5] Ha S T *et al* 2014 Synthesis of organic–inorganic lead halide perovskite nanoplatelets: towards high-performance perovskite solar cells and optoelectronic devices *Adv. Opt. Mater.* **2** 838–44

[6] Garreau A and Duvail J L 2014 Recent advances in optically active polymer-based nanowires and nanotubes *Adv. Opt. Mater.* **2** 1122–40

[7] Espinha A *et al* 2015 Random lasing in novel dye-doped white paints with shape memory *Adv. Opt. Mater.* **3** 1080–7

[8] Lau S P *et al* 2005 Flexible ultraviolet random lasers based on nanoparticles *Small* **1** 956–9

[9] Lawandy N M *et al* 1994 Laser action in strongly scattering media *Nature* **368** 436–8

[10] Polson R, Chipouline A and Vardeny Z V 2001 Random lasing in π-conjugated films and infiltrated opals *Adv. Mater.* **13** 760–4

[11] De Souza M, Lencina A and Vaveliuk P 2006 Lasing features in scattering gain media and amplified spontaneous emission systems *J. Appl. Phys.* **100** 023113

[12] Luan F *et al* 2015 Lasing in nanocomposite random media *Nano Today* **10** 168–92

[13] Wiersma D S 2008 The physics and applications of random lasers *Nat. Phys.* **4** 359–67

[14] Ambartsumyan R *et al* 1966 *ZhETF Pis. Red.* **3** 262
Ambartsumyan R *et al* 1966 *JETP Lett.* **3** 167

[15] Ghofraniha N *et al* 2015 Experimental evidence of replica symmetry breaking in random lasers *Nat. Commun.* **6** 6058

[16] Uppu R and Mujumdar S 2015 Exponentially tempered Lévy sums in random lasers *Phys. Rev. Lett.* **114** 183903

[17] Gomes A S *et al* 2016 Observation of Lévy distribution and replica symmetry breaking in random lasers from a single set of measurements *Sci. Rep.* **6** 27987

[18] Liu J *et al* 2014 Random nanolasing in the Anderson localized regime *Nat. Nanotechnol.* **9** 285–9

[19] Redding B, Choma M A and Cao H 2012 Speckle-free laser imaging using random laser illumination *Nat. Photon.* **6** 355–9

[20] Mermillod-Blondin A, Mentzel H and Rosenfeld A 2013 Time-resolved microscopy with random lasers *Opt. Lett.* **38** 4112–5

[21] Abegão L M *et al* 2016 Measuring milk fat content by random laser emission *Sci. Rep.* **6** 35119

[22] Ismail W Z W *et al* 2016 Dopamine sensing and measurement using threshold and spectral measurements in random lasers *Opt. Express* **24** A85–91

[23] Polson R and Vardeny Z V 2010 Cancerous tissue mapping from random lasing emission spectra *J. Opt.* **12** 024010

[24] Ferreira R, André P and Carlos L 2010 Organic–inorganic hybrid materials towards passive and active architectures for the next generation of optical networks *Opt. Mater.* **32** 1397–409

[25] Balachandran R, Pacheco D and Lawandy N 1996 Laser action in polymeric gain media containing scattering particles *Appl. Opt.* **35** 640–3

[26] Gomes A S *et al* 2014 Direct three-photon excitation of upconversion random laser emission in a weakly scattering organic colloidal system *Opt. Express* **22** 14305–10

[27] Marinho S *et al* 2015 Bi-chromatic random laser from alumina porous ceramic infiltrated with rhodamine B *Laser Phys. Lett.* **12** 055801

[28] Murai S *et al* 2010 Random lasing from localized modes in strongly scattering systems consisting of macroporous titania monoliths infiltrated with dye solution *Appl. Phys. Lett.* **97** 031118

[29] Sznitko L, Mysliwiec J and Miniewicz A 2015 The role of polymers in random lasing *J. Polym. Sci.* B **53** 951–74

[30] Sanchez C *et al* 2011 Applications of advanced hybrid organic–inorganic nanomaterials: from laboratory to market *Chem. Soc. Rev.* **40** 696–753

[31] Altman J *et al* 1991 Solid-state laser using a rhodamine-doped silica gel compound *IEEE Photonics Technol. Lett.* **3** 189–90

[32] Hu L and Jiang Z 1998 Laser action in Rhodamine 6G doped titania-containing ormosils *Opt. Commun.* **148** 275–80

[33] Zhu X-L, Lam S-K and Lo D 2000 Distributed-feedback dye-doped solgel silica lasers *Appl. Opt.* **39** 3104–7

[34] Pecoraro E *et al* 2010 Real time random laser properties of Rhodamine-doped di-ureasil hybrids *Opt. Express* **18** 7470–8

[35] García-Revilla S *et al* 2009 1Low threshold random lasing in dye-doped silica nano powders *Opt. Express* **17** 13202–15

[36] Alencar L D *et al* 2014 High fluorescence quantum efficiency of CdSe/ZnS quantum dots embedded in GPTS/TEOS-derived organic/silica hybrid colloids *Chem. Phys. Lett.* **599** 63–7

[37] Ferreira P *et al* 2015 Femtosecond laser fabrication of waveguides in rhodamine B-doped GPTS/TEOS-derived organic/silica monolithic xerogel *Opt. Mater.* **47** 310–4

[38] Awano C M *et al* 2012 Structure and growth kinetics of 3-glycidoxypropyltrimethoxysilane-derived organic/silica hybrids at different temperatures *J. Phys. Chem.* C **116** 24274–80

[39] Wen J and Wilkes G L 1996 Organic/inorganic hybrid network materials by the sol–gel approach *Chem. Mater.* **8** 1667–81

[40] Malucelli G *et al* 2005 Hybrid nanocomposites containing silica and PEO segments: preparation through dual-curing process and characterization *Polymer* **46** 2872–9

[41] Amerio E *et al* 2005 Preparation and characterization of hybrid nanocomposite coatings by photopolymerization and sol–gel process *Polymer* **46** 11241–6

[42] Takahashi M *et al* 2009 Self-organized nanocrystalline organosilicates in organic–inorganic hybrid films *Adv. Mater.* **21** 1732–6

[43] Malitson I 1965 Interspecimen comparison of the refractive index of fused silica∗ *Josa* **55** 1205–9

[44] Oliveira P W *et al* 1997 Generation of wet-chemical AR coatings on plastic substrates by the use of polymerizable nanoparticles *Optical Science, Engineering and Instrumentation'97* (International Society for Optics and Photonics)

[45] Enciso E *et al* 2010 Conventional unidirectional laser action enhanced by dye confined in nanoparticle scatters *Langmuir* **26** 6154–7

[46] Martín V *et al* 2011 Photophysical and lasing properties of rhodamine 6G confined in polymeric nanoparticles *J. Phys. Chem.* C **115** 3926–33

[47] Meng X *et al* 2008 Random lasers with coherent feedback from highly transparent polymer films embedded with silver nanoparticles *Appl. Phys. Lett.* **92** 201112

[48] Van Soest G, Tomita M and Lagendijk A 1999 Amplifying volume in scattering media *Opt. Lett.* **24** 306–8